Earth and Planetary Science Letters, 86 (1987) 240–252
Elsevier Science Publishers B.V., Amsterdam – Printed in The Netherlands

[6]

Rapid early Miocene acceleration of uplift in the Gangdese Belt, Xizang (southern Tibet), and its bearing on accommodation mechanisms of the India-Asia collision

Peter Copeland [1], T. Mark Harrison [1], W.S.F. Kidd [1], Xu Ronghua [2] and Zhang Yuquan [3]

[1] *Department of Geological Sciences, State University of New York at Albany, Albany, NY 12222 (U.S.A.)*
[2] *Institute of Geology, Academia Sinica, Postbox 634, Beijing (People's Republic of China)*
[3] *Institute of Geochemistry, Academia Sinica, P.O. Box 91, Guiyang (People's Republic of China)*

Received May 1, 1987; revised version received September 8, 1987

Five samples from a biotite-hornblende granodiorite phase of the 42.5 Ma Quxu pluton, Gangdese batholith, southern Tibet, have been collected at 250 m vertical intervals. Biotite from these rocks yields monotonically decreasing $^{40}Ar/^{39}Ar$ isochron ages with decreasing elevation of 26.8 ± 0.2, 23.3 ± 0.5, 19.7 ± 0.3, 18.4 ± 0.4, and 17.8 ± 0.1 Ma ($T_c = 335\,^\circ$C). Coexisting K-feldspars have virtually identical minimum apparent $^{40}Ar/^{39}Ar$ ages of 17.0 ± 0.4 Ma ($T_c = 285\,^\circ$C). These data indicate parts of southern Tibet experienced a pulse of uplift in the early Miocene with the rate of uplift rising from 0.07 to ~ 4.4 mm/year in the interval 20 to 17 Ma. An apatite fission track age of 9.9 ± 0.9 Ma from this locality constrains the average uplift rate at this site to about 0.81 mm/year between 17 and 9.9 Ma and 0.30 mm/year from 9.9 Ma to present. K-feldspar from the Dagze granite, 30 km to the east, near Lhasa, yields a minimum apparent $^{40}Ar/^{39}Ar$ age of 35.9 ± 0.9 Ma ($T_c = 227\,^\circ$C) which indicates an average uplift rate there of 0.21 mm/year since then. The marked pulse of uplift of the Quxu granodiorite and the difference in uplift history between the Dagze and Quxu plutons suggests southern Tibet has experienced discrete pulses of uplift variable in both space and time. These data are not consistent with models which require a large proportion of uplift of the Tibetan plateau to have occurred in the last 2 Ma. The data support the suggestion that convergence between India and Asia was largely accommodated by tectonic escape during the opening of the South China Sea 32 to 17 Ma ago and permit distributed shortening as a mechanism for crustal thickening and uplift of this part of the Tibetan plateau subsequent to 20 Ma.

1. Introduction

The Tibetan plateau and the Himalayas, produced by the collision of India with Asia, are the most prominent example of a contemporary large-scale continent-continent collision. Despite the obvious topographic manifestations of this collision, many questions remain regarding the nature and rates of the mechanisms that produced these features. We here present $^{40}Ar/^{39}Ar$ and fission track mineral ages from rocks of the Gangdese batholith, southern Tibet, and our conclusions from these data regarding uplift rates and crustal shortening and thickening mechanisms in southern Tibet since the collision began.

The geologic boundary between Asia and India is the Indus-Zangbo suture zone (Fig. 1). This suture is marked by the presence of ophiolites [1] which are the remnants of thousands of kilometers of oceanic crust of the Tethys Ocean which was subducted beneath Asia before the India-Asia collision. The the north of the suture lies the Gangdese (Transhimalayan) batholith (Fig. 1). This is a large I-type [2] composite batholith with an average composition of granodiorite [3]. Before the India-Asia collision, the Gangdese Belt was an active Andean-type continental-margin arc at the southern edge of Asia. Crystallization ages in the Gangdese range from 110 to 40 Ma [4,5]. The India-Asia collision had begun by about 40 Ma based on a slowdown of the convergence rate derived from marine magnetic anomalies [6] and the age of the youngest plutons in the Gangdese Belt [4]. Some authors maintain that the collision began earlier at about 50 Ma [7,8]. Since 40 Ma, approximately 2000 km of convergence has taken place [9,10]. Tectonic accommodation of convergence has occurred by some mix of approximately

0012-821X/87/$03.50

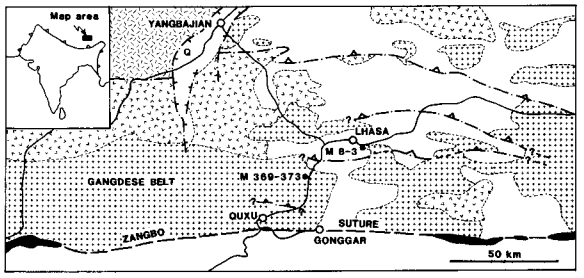

Fig. 1. Simplified geologic map of the southern Lhasa terrane in the vicinity of Lhasa. Continuous lines = roads; dot-dash lines: with ticks = normal faults; with triangles = thrust faults; + symbols = Gangdese batholith; V symbols = Paleogene volcanic rocks; random dash symbols = granitoid gneisses; black = ophiolites; blank = Carboniferous to Cretaceous sedimentary and volcanic rocks; Q = Quaternary of Yangbajian graben; sample localities discussed in this paper shown by black dots. Geology from Ministry of Geology [66], Burg et al. [50], and observations by members of the 1985 Academia Sinica—Royal Society Geotraverse [31]. For cross-sections in this area see Burg et al. [50], and Burg [67]. Line with triangles on inset map is the southern edge of the Himalaya (MBT).

north-south crustal shortening (and thickening) [11,12], and by largely eastward tectonic escape using large-displacement strike-slip fault zones [6,13,14], east-west extension on approximately north-south trending normal faults has also been a less major tectonic result of the collision [15]. Our results have implications for the relative contribution of crustal shortening and tectonic escape at different times in the past 40 Ma. They can also help discriminate between different mechanisms of crustal shortening proposed to account for the twice-normal thickness continental crust of the Tibetan plateau if, as seems likely, uplift is connected directly with thickening.

2. Experimental procedures

High purity mineral separates were obtained by standard mineral separation techniques. Sample preparation, irradiation, and $^{40}Ar/^{39}Ar$ isotopic analyses followed the procedures of Harrison and FitzGerald [16]. Correction factors used to account for interfering nuclear reactions were $(^{39}Ar/^{37}Ar)_{Ca} = 8.25 \times 10^{-4}$, $(^{36}Ar/^{37}Ar)_{Ca} = 2.22 \times 10^{-4}$, and $(^{40}Ar/^{39}Ar)_K = 0.029$. Results of $^{40}Ar/^{39}Ar$ analyses are available from the authors upon request. All quoted errors are at one sigma.

Kinetic parameters required for biotite closure temperature (T_c) calculations [17] have been determined using an isothermal-hydrothermal heating experiment in conjunction with an existing Ar diffusion law. Biotite from sample M373 together with approximately 10 wt.% water was sealed in a Pt capsule and treated at $710 \pm 5\,^{\circ}C$ and 1 kbar in a cold seal bomb for 141.8 hours. Both a sample of the untreated and the hydrothermally heated material were then analyzed to determine the fraction of radiogenic ^{40}Ar ($^{40}Ar^*$) lost during heating. Using an infinite cylinder diffusion model (see [18,19]) and the observed loss allows calculation of a D/a^2 value, the diffusion coefficient/grain size parameter. The average grain radius of the biotite used in this experiment is 0.8 ± 0.2 mm. Because the diffusivity of Ar has been found to vary with composition in the annite-phlogopite series [19], the composition of the biotite from M373 was determined by electron microprobe to be 49 mol% annite. This is taken to be the composition of biotite in the rest of our samples from the Quxu granodiorite. Harrison et al. [19] have shown that biotites of approximately this composition have an activation energy of 47 kcal/mol. The fractional loss of $^{40}Ar^*$ in this experiment of 7.8% translates to a D/a^2 value of 2.4×10^{-9}/s. This activation energy and our calculated D/a^2 value correspond to a D_0/a^2 (frequency factor/grain size parameter) of 68/s, implying an effective diffusion radius of 0.34 mm (see [19]). Using this value and an assumed cooling rate through the closure interval of $10\,^{\circ}C$/Ma, we calculate a closure temperature of $335 \pm 15\,^{\circ}C$ for the biotite from sample M373 which we take to be the closure temperature for biotite in all of our samples from this granodiorite pluton.

Intrinsic Ar diffusion parameters fr the K-feldspars have been determined using the approach of Harrison and McDougall [20]. Diffusion coefficients are calculated from measured ^{39}Ar loss during laboratory heating. A plot of these values against the reciprocal absolute temperature of heating reveals the Arrhenius parameters; activation energy (E) and frequency factor/grain size (D_0/a^2).

The apatite fission-track age was obtained using the external detector method and followed the procedures of Baldwin et al. [21] and Naeser [22]. Neutron dose was determined via NBS SRM 962 glass, calibrated using Fish Canyon apatite [23].

3. The Gangdese Belt

The Gangdese batholith is a semi-continuous belt of plutons which stretch out over 2600 km along strike [3]. Most workers have argued for an Andean-type continental-margin setting for the batholith (e.g. [24]). Others have suggested an intra-oceanic island arc, later accreted to Asia, as the tectonic setting for the Gangdese Belt [25]. Isotopic data suggest a largely mantle source for the rocks of the Gangdese, with small amounts (< 30%) of crustal assimilation [3,26].

3.1 Quxu pluton

We have sampled a portion of the Quxu composite pluton, a biotite-hornblende granodiorite (A2 unit of Debon et al. [3]) at a location adjacent to the highway about 24 km southwest of Lhasa (Fig. 1). Accessory minerals include sphene, epidote, apatite, zircon, and magnetite-ilmenite. Details of petrography and geochemistry of this pluton can be found in Debon et al. [3]. Five samples (M369–373) were collected at 250 m vertical intervals along a 3 km traverse from 3.6 to 4.6 km above sea level at this locality on the west side of the Quxu (Lhasa) River valley. Outcrop is good and there are no shear zones or other evidence for major differential movement between sample sites.

In order to estimate the depth of crystallization of the Quxu pluton we have determined the composition of hornblende in sample M373 by electron microprobe. This hornblende has 1.5 total Al per 23 oxygens. Using the geobarometer of Hammarstrom and Zen [27,28] this translates into a depth of 13 ± 3 km below the surface ($\rho = 2.85$ g/cm^3).

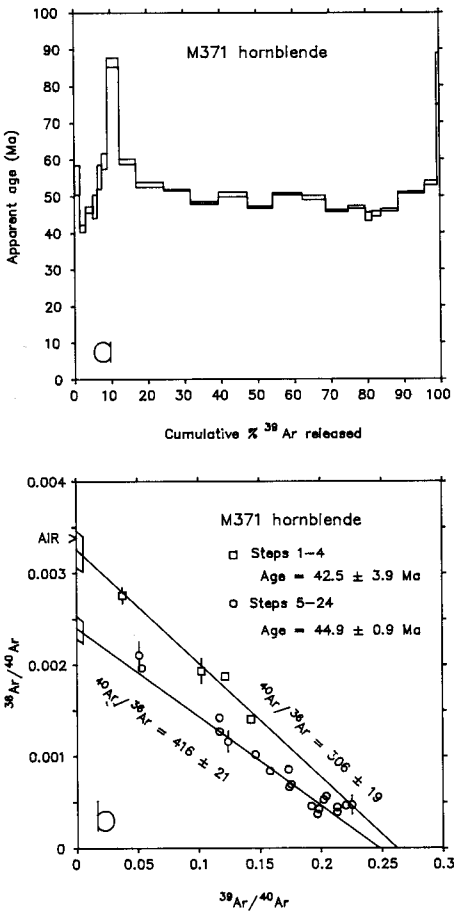

Fig. 2. (a) $^{40}Ar/^{39}Ar$ age spectrum diagram for hornblende from sample M371. This approach assumes initial $^{40}Ar/^{36}Ar = 295.5$. (b) Ar isotope correlation diagram for this sample showing two trapped components of 306 ± 19 and 416 ± 21 which are thermally distinct during laboratory heating. The ages from the two regressions are indistinguishable within uncertainty.

TABLE 1

Result of Ar isotope isochron analysis for hornblendes from the Quxu pluton

Sample	Number of steps	% of ^{39}Ar released	Age (Ma)	$(^{40}Ar/^{36}Ar)_i$	MSWD
M369	3	35.5	43.8 ± 10.4	281 ± 131	2.5
	5	33.4	40.7 ± 0.7	507 ± 13	0.4
M370	14	96.3	46.4 ± 0.4	378 ± 7	16
M371	4	6.6	42.5 ± 3.9	306 ± 19	9.8
	19	93.4	44.9 ± 0.9	416 ± 21	32
M372	5	5.7	37.8 ± 7.7	366 ± 12	5.7
	20	94.0	42.0 ± 0.9	458 ± 20	18
Average age			43.5 ± 0.7		

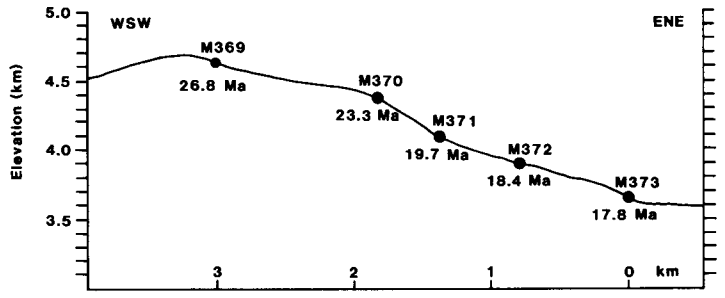

Fig. 3. Topographic profile of the field traverse in the Quxu pluton. Ages by sample sites are $^{40}Ar/^{39}Ar$ isochron ages from biotites (see Table 2). No vertical exaggeration.

$^{40}Ar/^{39}Ar$ analysis on hornblendes from four of our samples from the Quxu pluton (samples M369–372) give complex saddle-shaped release spectra with irregular patterns. These results can be explained with reference to isotope correlation diagrams. Isochron analysis indicates multiple trapped Ar components which are largely thermally distinct during laboratory heating. $^{40}Ar/^{36}Ar$ compositions—as high as 500 (sample M369)—readily explain the complex age spectra for these minerals [29]. The results of isochron analysis are shown in Table 1. Fig. 2 illustrates an example of this phenomenon in sample M371. The first four heating steps, which comprise 6.6% of the ^{39}Ar released, define a line on the isochron diagram (Fig. 2b) with intercepts that correspond to an age of 42.5 ± 3.9 Ma and a trapped component with a $^{40}Ar/^{39}Ar$ composition of 306 ± 19, indistinguishable from the atmospheric value of 295.5. Steps 5–24, which comprise the remaining 93.4% of the ^{39}Ar released, define a linear trend that corresponds to an age of 44.9 ± 0.9 Ma and a trapped component with a $^{40}Ar/^{36}Ar$ equal to 416 ± 21. Using this trapped component rather than 295.5 would yield a plateau in Fig. 2a at 45 Ma as opposed to the scatter of values shown from 88 to 46 Ma. The average age of the four hornblendes from the Quxu pluton is 43.5 ± 0.7 Ma (Table 1). Schärer et al. [4] have analyzed zircons from two samples of this pluton, taken near the village of Quxu (Fig. 1) about 25 km southwest of localities M369–373, which yield concordant U-Pb ages of 41.1 ± 0.4 and 41.7 ± 0.4 Ma. While the U-Pb zircon and $^{40}Ar/^{39}Ar$ hornblende ages do overlap at 2σ, the contrast in age may be due to minor radiogenic Pb loss from the zircons or imprecision in isochron analysis reflected by the generally high MSWD (Table 1) resulting from minor mixing of trapped Ar components during experimental evolution of the gas. We take the crystallization age of this body to be 42.5 ± 1.5 Ma.

Ages for the Quxu biotites have been calculated by the isochron method. This analysis yields monotonically decreasing ages with decreasing elevation of 26.8 ± 0.2, 23.3 ± 0.5, 19.7 ± 0.3, 18.4 ± 0.4, and 17.8 ± 0.1 Ma (Table 2). Not only do the ages of these biotites decrease systematically with decreasing elevation but the difference between the ages of successive samples also de-

TABLE 2

Results of Ar isotope isochron analysis of biotites from the Quxu pluton

Sample	Number of steps	% of ^{39}Ar released	Total fusion age for this interval (Ma)	Apparent age from isochron (Ma)	($^{40}Ar/^{36}Ar$)	MSWD
M369	10	92.7	27.1	26.8±0.2	327±65	95
M370	11	88.9	22.8	23.3±0.5	278±11	24
M361	9	92.2	19.9	19.7±0.3	322±41	12
M372	9	91.4	18.4	18.4±0.4	293±11	8.6
M373	9	95.7	18.1	17.8±0.1	317±10	4.0

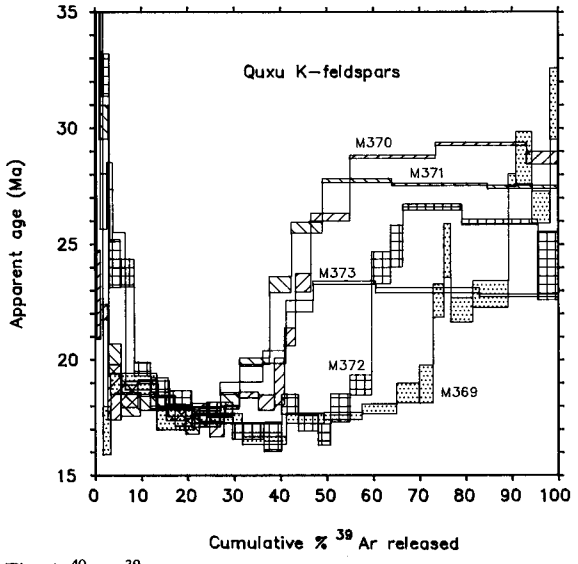

Fig. 4. $^{40}Ar/^{39}Ar$ age spectra analyses of K-feldspars from the Quxu pluton.

creases downward. Fig. 3 is a topographic profile of the field traverse with these biotite ages shown next to the sample sites. As with the hornblendes, isochron analysis of three of the five of the Quxu biotites analyzed reveals a non-atmospheric trapped Ar composition. Details of these isochron analyses are given in Table 2.

In Fig. 4, $^{40}Ar/^{39}Ar$ age spectra for K-feldspars from the five Quxu samples are shown. These five

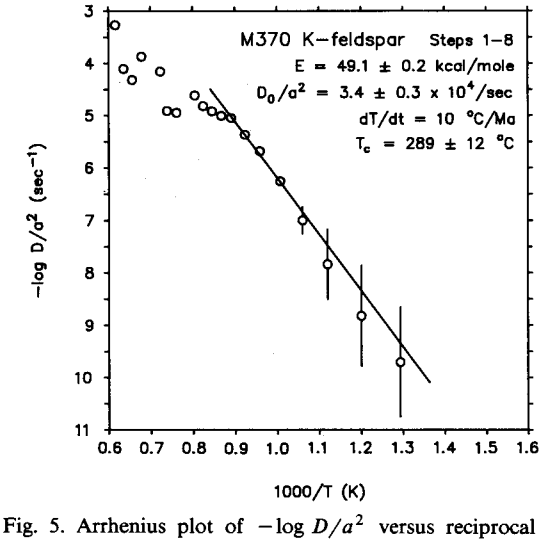

Fig. 5. Arrhenius plot of $-\log D/a^2$ versus reciprocal absolute temperature for K-feldspar from sample M370. Arbitrary uncertainties assigned based on amount of gas present.

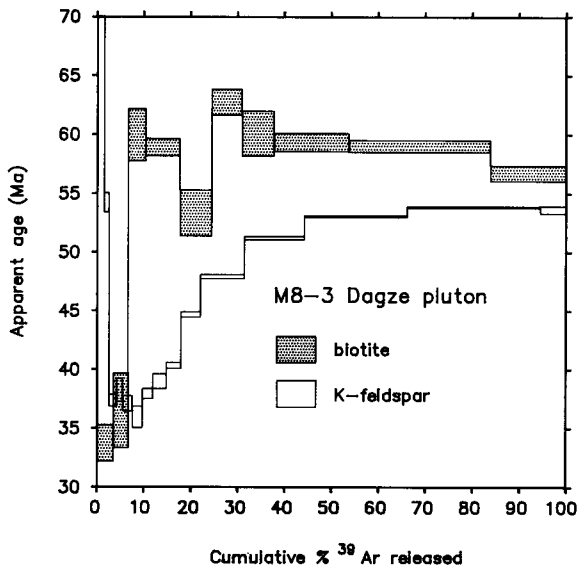

Fig. 6. $^{40}Ar/^{39}Ar$ age spectra analyses of biotite and K-feldspar from sample M8-3, Dagze pluton. Isochron analysis of this biotite gives an age of 58.4 ± 2.2 Ma and a trapped $^{40}Ar/^{36}Ar$ composition of 471 ± 73.

minerals have virtually identical minimum apparent ages at about 20% ^{39}Ar release, which have an average value of 17.0 ± 0.4 Ma. The calculated closure temperature for this portion of Ar release, obtained from internally derived kinetic parameters [17,20], is 285–15 °C, assuming a cooling rate of 10 °C/Ma through the closure isotherm. The uncertainty in closure temperature reflects the internal variation (1 s.d.) of the three K-feldspars that yield systematic Arrhenius variations. Activation energies obtained (48.8 ± 0.2 kcal/mol) are similar to that reported by Foland [30]. Arrhenius results for sample M370, which has a closure temperature of 289 ± 12 °C, are shown in Fig. 5. The two samples which show greater scatter on Arrhenius diagrams (M369 and M371) yield lower, but less well constrained closure temperatures. Differences in the age spectra of the Quxu K-feldspars are due to variable amounts of excess ^{40}Ar in the early portion of gas release and variable maximum closure temperature in the later portion of gas release. The late portions of gas release yield ages greater than ages of coexisting biotite, indicating portions of these K-feldspars are more retentive than the biotite.

Sample M370 gives an apatite fission-track age of 9.9 ± 0.9 Ma.

3.2. Dagze pluton

Another pluton of the Gangdese Belt was sampled near Lhasa (Fig. 1). This rock (M8-3), from the edge of the Dagze pluton, is a biotite granite in which the biotite has been partially altered to chlorite. Fig. 6 shows the $^{40}Ar/^{39}Ar$ release spectra for biotite and K-feldspar from this sample. Isochron analysis reveals an age for the plateau portion of the biotite spectra of 58.4 ± 2.2 Ma and a trapped component with a $^{40}Ar/^{36}Ar$ equal to 471 ± 73. This places a constraint on the minimum age of this body. No U-Pb zircon ages are presently available for the Dagze pluton. The early portion of gas release (approximately the first 3%) for the K-feldspar is dominated by excess Ar. The minimum apparent age for the K-feldspar from this rock is 35.9 ± 0.9 Ma. Because of the potential for excess Ar to be present in all gas fractions analyzed, this age is regarded as a maximum estimate of the time the K-feldspars reached their closure temperature, which is 227 ± 15 °C for an assumed cooling rate through the closure interval of 10 °C/Ma. The difference in closure temperature for the K-feldspar of the Quxu and Dagze plutons can be explained by differences in crystal structure (see [20]).

4. Uplift rates

Uplift rates can be calculated from thermochronologic data by three approaches. The first is by obtaining the ratio of the difference in elevation between two identical minerals and the difference in their mineral ages. This method assumes that the closure temperature is the same for both minerals, that they passed upward through stationary isotherms, and that the geothermal gradient remained constant during the interval between the times these minerals reached their closure temperatures. The second approach utilizes two mineral ages from the same sample, in this case either biotite/K-feldspar or K-feldspar/apatite. By dividing the ratio between the difference in closure temperatures and the difference in mineral age by an assumed geothermal gradient, an average uplift rate for the interval between the two mineral ages is obtained. The third approach of calculating uplift rates is to divide a known amount of uplift by the duration over which the uplift took place. Depths can be determined by using a geobarometer, such as Al in hornblende mentioned above, or by taking a mineral closure temperature and dividing by a geothermal gradient to obtain the depth below the surface of the earth at the time the mineral reached its closure temperature. In this discussion, no error is assigned to the choice of geothermal gradient. Errors in depth assignment will arise from either the inherent error associated with the geobarometer or the uncertainty in estimation of the closure temperature. All rocks in this study were collected at known elevations on the earth's surface, providing the final datum in depth-time space.

4.1. Quxu pluton

Using these approaches, uplift rates for the Quxu granodiorite have been calculated for several time intervals (Table 3, Fig. 7).

The Al geobarometer [27,28] places sample M373 at ~ 13 km below the surface at 42.5 Ma, the time of crystallization given by the $^{40}Ar/^{39}Ar$ hornblende and U-Pb zircon ages. Taking the experimentally determined closure temperature of the Quxu biotites of 335 °C, we can place sample M369 (now 1 km above M373) at 11.2 km below the surface at 26.8 Ma, given an assumed geothermal gradient of 30 °C/km. This corresponds to

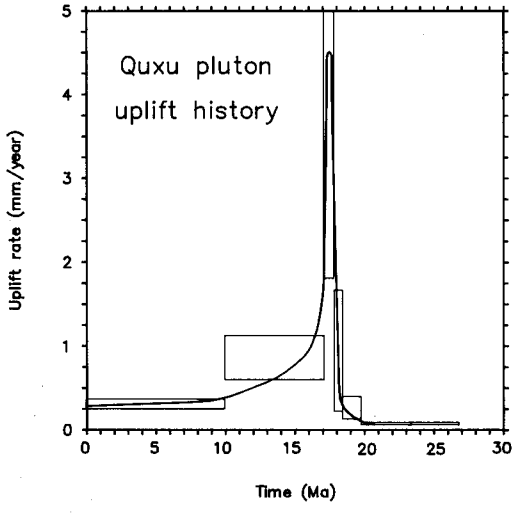

Fig. 7. Uplift history of the Quxu pluton for the last 30 Ma as given by $^{40}Ar/^{39}Ar$ and fission-track mineral ages. Boxes reflect uncertainty in uplift rate for individual time intervals (see Table 3). Uplift rate for the interval 17.8 to 17.0 Ma is $4.4 \pm {}^{17.1}_{2.6}$ mm/year.

TABLE 3

Mineral ages and calculated uplift rates for the Quxu pluton

Sample	Elevation (m a.s.l.)	Mineral	T_c (°C)	Depth (km) [a]	Apparent age (Ma)	Average uplift rate (mm/year)
M373	3600 ± 5	hornblende, zircon [f]		~13.4	42.5 ± 1.5	
M369	4600 ± 10	biotite	335 ± 15	11.2 ± 0.5 [b]	26.8 ± 0.2	~0.07
						$0.07 \pm {}^{0.02}_{0.01}$
M370	4350 ± 10	biotite	335 ± 15	11.2 ± 0.5 [b]	23.3 ± 0.5	$0.07 \pm {}^{0.02}_{0.01}$
M371	4100 ± 15	biotite	335 ± 15	11.2 ± 0.5 [b]	19.7 ± 0.3	
						$0.20 \pm {}^{0.20}_{0.07}$
M372	3850 ± 15	biotite	335 ± 15	11.2 ± 0.5 [b]	18.4 ± 0.4	
						$0.39 \pm {}^{1.28}_{0.17}$
M373	3600 ± 5	biotite	335 ± 15	11.2 ± 0.5 [b]	17.8 ± 0.1	
						$4.4 \pm {}^{17.1}_{2.6}$ [d]
M369-M373	4600-3600	K-spars	285 ± 15	7.7 ± 0.4 [c]	17.0 ± 0.4	
						$0.81 \pm {}^{0.31}_{0.21}$ [e]
M370	4350 ± 10	apatite	90 ± 10	3.0 ± 0.3 [b]	9.9 ± 0.9	
						$0.30 \pm {}^{0.07}_{0.05}$
Surface of earth			0	0	0	

[a] Uncertainties reflect analytical uncertainty of geobarometer or error in closure temperature.
[b] Based on an assumed geothermal gradient of 30 °C/km.
[c] Based on an assumed geothermal gradient of 37 °C/km.
[d] Calculated by area balance method.
[e] Based on an assumed geothermal gradient of 34 °C/km.
[f] See text discussion for zicon sample location [4].

an uplift relative to the surface of the earth of ~1 km in the interval 42.5 to 26.8 Ma at an average rate of about 0.07 mm/year. We think 30 °C/km is an appropriate estimate for a geothermal gradient in an orogenic terrane (e.g. [31]). If the geothermal gradient in the Quxu area was different from this value in the interval 45 to 20 Ma, the absolute values of uplift rate calculated here would be changed correspondingly. This would not, however, alter the relative changes in uplift rates shown in Fig. 7. The shape of the curve in Fig. 7, not its specific location, forms the basis of our conclusions. Non-systematic variations in closure temperatures of biotite and would vary to a small extent both the shape and location of the portion of this curve defined by the biotite data, between 27 and 17.8 Ma.

For the period from 27 to 18 Ma uplift rates are calculated using the differences in age and elevation of the five biotites (Table 3). From 27 to 19.7 Ma the area experienced constant and relatively slow uplift of $0.07 \pm {}^{0.02}_{0.01}$ mm/year. Over the interval 19.7 to 18.4 Ma the uplift averaged $0.20 \pm {}^{0.20}_{0.07}$ mm/year and from 18.4 to 17.8 the uplift rose to a rate of $0.39 \pm {}^{1.28}_{0.17}$ mm/year.

Using the closure temperature of 335 °C, obtained from the hydrothermal heating experiment described in section 2, together with the estimate of the geothermal gradient of 30 °C/km, we can place the lowermost sample at a depth of 11.2 km below the surface at ca. 17.8 Ma. Since these rocks are now at the surface, we require a minimum average rate of uplift for the Quxu pluton subsequent to 17.8 Ma of 0.63 mm/year.

The observation that all five K-feldspars yield apparent age minima of approximately 17 Ma, which corresponds to a closure temperature of 285 °C, indicates that our 1 km vertical section of crust passed through the K-feldspar closure isotherm very rapidly. To use the same method to calculate uplift rate used for the biotite above would give an infinite rate of uplift. The contrasts in age and closure temperature of biotite from sample M373 and the K-feldspars gives an average uplift rate of $2.1 \pm {}^{11.2}_{1.6}$ mm/year for the interval 17.8 to 17.0 Ma, given a geothermal gradient of 30 °C/km. However, to continue to use 30 °C/km as the geothermal gradient after an episode of uplift more rapid than about 0.2 mm/year is inappropriate as the isotherms will begin to be significantly perturbed upwards, creating a steeper geothermal gradient (e.g. [32]). In order to evaluate

the magnitude of this effect we have calculated the first-order thermal consequences of the uplift history given above for the interval 20 to 17 Ma using a one-dimensional numerical heat flow model [33]. The very slow uplift phase prior to 20 Ma ($\sim$ 0.07 mm/year) has been neglected because of the trivial disturbance of the isotherms [32]. This calculation suggests a geothermal gradient of 37 °C/km for the Quxu pluton at 17 Ma given an initial value of 30 °C/km at 20 Ma. The $2.1 \pm {}^{11.2}_{1.6}$ mm/year rate is reduced to $1.7 \pm {}^{9.1}_{1.3}$ mm/year when this geothermal gradient is used.

Another method provides an alternative result for the uplift rate for this interval. By taking a geothermal gradient of 37 °C/km, these K-feldspars can be placed at a depth of approximately 7.7 km by 17 Ma, and thus an average post-17 Ma uplift rate of 0.45 mm/year is required. Knowing the uplift rates intervals 17.8 Ma–present and 17 Ma–present allows us to infer the average uplift rate for the interval 17.8 to 17 Ma. This is done by calculating the 17.8 to 17 Ma uplift rate that will balance the "uplift deficit" created by 17 Ma of 0.45 mm/year uplift to yield an integrated average uplift rate over the past 17.8 Ma of 0.63 mm/year. The necessary average uplift rate for 17.8 to 17 Ma is $4.4 \pm {}^{17.1}_{2.6}$ mm/year, which compares well with the uplift rate calculated above directly from the K-feldspar/biotite couple of $1.7 \pm {}^{9.1}_{1.3}$ mm/year. We choose this result for the interval 17.8 to 17.0 Ma because it includes the constraint that the rocks are at the surface today. The minimum rate allowed by this result for this interval is more than 2.5 times greater than the average post-17.8 Ma rate of 0.63 mm/year and therefore requires an acceleration of uplift rate during the interval 17.8 to 17.0 followed by a deceleration to lower rates in the post-17 Ma interval.

While the post-17 Ma average uplift rate is given by the age and closure temperature of the K-feldspars, the details of this portion of uplift history are constrained by the apatite fission-track age of sample M370. The geothermal gradient would have relaxed to its equilibrium value of 30 °C/km by 9.9 Ma, the apatite fission-track age. Given that the average geothermal gradient for this region between 17 and 10 Ma was 34 °C/km and our knowledge of the apatite fission-track closure temperature of 90 ± 10 °C [34,35], we calculate the average uplift rate between the closure of the K-feldspars (17 ± 0.4 Ma) and apatite (9.9 ± 0.9 Ma) to be $0.81 \pm {}^{0.31}_{0.21}$ mm/year. This closure temperature and a geothermal gradient of 30 °C/km places this sample at a depth of 3 km by 9.9 Ma requiring an average uplift rate of $0.30 \pm {}^{0.07}_{0.05}$ mm/year to the present day (Table 3).

The uplift history of the Quxu granodiorite is summarized in Fig. 7. A remarkable feature of these data is that they document both the acceleration and deceleration of a brief episode of very rapid uplift. The tectonic implications of such an uplift history are discussed below.

4.2. Dagze pluton

Using an assumed geothermal gradient of 30 °C/km, a closure temperature of 310 °C for biotite [19], and our calculated closure temperature of 227 °C for K-feldspar, we can place the sample from the Dagze granite, near Lhasa, at $\sim$ 10.3 km below the surface at ca. 58 Ma and $\sim$ 7.6 km below the surface at ca. 36 Ma. From these data we calculate an average uplift rate of 0.14 mm/year for the interval 58 to 36 Ma and 0.21 mm/year from 36 Ma to the present.

5. Discussion

Convergence between India and Asia is accommodated largely by crustal shortening and strike-slip faulting (tectonic escape); some N-S trending extensional faulting also results. Details of and evidence for these mechanisms have recently been reviewed by Tapponnier et al. [36]. The conspicuous elevation and crustal thickness of the Tibetan plateau has been suggested to be a product of distributed crustal shortening [11,37–40], continental underplating or underthrusting [41–44], or injection of magma into or at the base of the Tibetan crust [45–47]. The uplift history of the Quxu granodiorite derived from the mineral ages presented here places quantitative constraints on the timing and the mechanisms of crustal uplift and thickening in southern Tibet.

Fig. 7 shows the uplift history of the Quxu pluton to be marked by a sharp pulse of uplift to a maximum of about 4.4 mm/year in the interval 20 to 17 Ma. This represents a sixty-fold increase in rate of uplift in less than 3 Ma. Zeitler [48] has observed a similar, but less dramatic, increase in

uplift rate in the northwest Himalayas at about 18 Ma. In the calculations to determine uplift rates it has been assumed that all samples have experienced the same amount of vertical uplift. If the lower samples have experienced slightly more vertical movement than the samples from higher elevations, thus creating a rotation of the block, the effect would be to increase the values of uplift rate in Fig. 7 and Table 3 which involve the samples from the lower part of the section. The Paleogene Linzizong volcanic units which lie to the north of the Gangdese belt (Fig. 1) are a calc-alkaline sequence coeval with at least part of the Gangdese [49]. This suggests any regional rotation in this area is likely to be about an east-west axis bringing the southern Gangdese up relative to the volcanic rocks to the north. Such a rotation would have little effect on our samples of the Quxu as our field traverse is ENE–WSW.

A potential criticism of this result is that our method gives information related to unroofing and is not a direct reflection of uplift with respect to an external reference. For example, erosion unaccompanied by differential crustal movements associated with orogeny could mimic the cooling history observed for the Quxu pluton. We can confidently rule this out in our case as we have considerable control on the fine-scale displacement of isotherms in the period 40 to 20 Ma. It is clear that approximately 3 km of erosion occurred in the late Oligocene/early Miocene. Our reconstruction places the peak of erosion at about 18 Ma. Although the pulse of uplift responsible for this erosion may have occurred earlier, we can constrain this contrast in time via simple thermal considerations. The uniformly low unroofing rates calculated from the two biotites of the shallowest samples are sensitive indicators of isotherm distribution in the late Oligocene. The response time of the 335 °C isotherm to movements on the order of the vertical separation of our samples following rapid uplift of 3 km (accompanied by erosion) is less than 200,000 years. Even in the case where erosion has occurred at a rate ten times less than uplift, the difference between the age of uplift and the onset of erosion would be only 2 Ma.

The sample of biotite granite collected near Lhasa, about 30 km along strike of the Gangdese belt, has had a different thermal history than the samples of the Quxu granodiorite. Although we do not have as much control on the changes in uplift rate of this body as we do for the Quxu pluton, it seems likely that, since the time the Quxu granodiorite crystallized (42.5 Ma), the Dagze granite has experienced relatively slow uplift with few excursions of uplift rate above the average post-36 Ma value of 0.21 mm/year. This suggests a structural discontinuity between these two nearby plutons.

The thermochronologic data cannot discriminate between pure vertical block uplift and a vertical component along a thrust fault or faults. Many faults probably exist in this area, but the only one mapped at present that projects between our two sample sites (Fig. 1) is a north-dipping fault mapped by Burg et al. [50] as a thrust, and cut by the Gangdese plutonic rocks. In order for this structure to be responsible for the differences in thermal history between the Quxu and Dagze samples, it would have to have had a normal, down-to-the-north displacement at some time(s) in the past 40 Ma, in addition to any earlier thrusting, and would have to cut the Gangdese plutons. Given the reconnaissance state of mapping in this area at present, another one or more unidentified structures, possibly a south-dipping thrust, is just as likely to be the locus of differential motion. We point out that the sense of the required differential motion is the same as that of the backthrusting known from near the Zangbo suture, which involves continental red arenites and conglomerates of probable Cenozoic age (Liuqu conglomerate, Luopusar Group, etc.) [50–52].

Many workers have concluded on the basis of paleobotanical and paleontological evidence [53–56] that major uplift of the Tibetan plateau did not occur until the Quaternary (e.g. [44,47,57]). We feel there are three potential problems with attempting to understand the uplift history of the Tibetan plateau by this approach. First, many of these studies are from the central part of the Tibetan plateau, whereas most of the deformation associated with uplift occurs at the margins [36,40]. Indeed, one such study that included samples from the southern margin of the plateau [58] concluded that "uplift of the plateau has been unbalanced and asymmetrical" and first accelerated in the early Miocene. Second, the composition of floral and faunal assemblages is largely a function of climate but elevation is only one of several

factors that influence climate. Thirdly, age assignment of non-marine strata is not usually highly precise and it would therefore be difficult to recognize or date accurately a brief pulse of uplift such as the one documented for the Quxu pluton. If, however, these studies are taken at face value, they are not strictly comparable to the thermochronologic data presented here. The paleobotanical data measure motion relative to sea level whereas the isotopic and fission-track data record motion relative to the surface of the earth. Therefore we again see that the uplift history shown in Fig. 7 is a minimum. The total uplift could be obtained by taking the sum of the uplift based on the two approaches. Powell [44] has proposed a model for the uplift and thickening of the Tibetan plateau in which Indian continental crust and lithosphere is postulated to have been subducted at a 45 degree angle beneath Tibet from 20 to 5 Ma. This continental crust is then thought to have become delaminated from the rest of the downgoing material and rapidly risen to the base of the Tibetan crust, moving aside the sub-Tibetan mantle. This model predicts that uplift of the Tibetan plateau did not begin until about 2 Ma with uplift being "more or less synchronous across the plateau". Zhao and Morgan [45,46] and Zhao and Yuen [47] have presented variations on a model of plateau formation in which an Indian crust is injected into the "fluid-like" Tibetan lower crust to produce "a steady rise of Tibet from middle Miocene to its present elevation". The model of Zhao and coworkers [46,47] assumes a constant or lognormal viscosity distribution and sets the maximum allowable viscosity in the Tibetan crust such that the greatest relief on the plateau would be 0.5 km. There are many examples from the interior as well as the margins of the plateau where relief exceeds 1 km. Indeed, the Nyainqentanglha range, approximately 100 km northwest of Lhasa, has topographic relief in excess of 2 km. Such topography suggests a heterogeneous rather than uniform viscosity distribution. The data presented here and our unpublished work in progress do not support these hypotheses. The spike in the uplift rate of the Quxu pluton at about 18 Ma and the sharp difference between the thermal histories of the Quxu and Dagze plutons suggest discrete pulses of uplift which are separated in space and time.

Li et al. [57] have proposed a model in which the Tibetan plateau has experienced a two-stage history of thickening and uplift. They suggest that, from Late Eocene to Pliocene, compressional deformation resulted in significant shortening and thickening and a deep, broad root in isostatic disequilibrium. This root then rose beginning in the Early Pleistocene, creating the Tibetan plateau. Our data suggest Eocene-Miocene shortening and thickening is a plausible scenario but that uplift was coincident with shortening rather than delayed by up to 20 Ma. Distributed shortening by folding and low-angle thrusting has been suggested to be a major mechanism of crustal thickening and uplift since the India-Asia collision began [11,37–40]. While they do not prove this model, our data are consistent with thickening and uplift by distributed shortening, particularly since 20 Ma ago.

Tapponnier et al. [36,59] have presented a model in which the opening of the South China Sea is a consequence of tectonic escape of southeastern China and movement along the Red River Fault. They observe that spreading rates during the period of sea-floor formation (32 to 17 Ma) were roughly equal to the convergence rate between India and Asia and conclude that, during this time, most if not all of the convergence was accommodated by tectonic escape along large-scale strike-slip faults. They further suggested that, as a consequence, uplift and thickening of the Tibetan plateau occurred prior to 32 Ma or after 17 Ma. The uplift history from the Quxu samples shown in Fig. 7, is consistent with such a scenario. Before 20 Ma, uplift was slow and constant. During the waning of spreading in the South China Sea (20 to 17 Ma) uplift in the Quxu region accelerated to a peak value of about 4.4 mm/year. We suggest this is evidence for a continuum of convergence accommodation mechanisms in eastern Asia. The deceleration of uplift in the Quxu region may be the result of another change in convergence accommodation mechanism or this deceleration may reflect the elevation produced by the new mechanism achieving isostatic equilibrium.

The time of first movement on the Main Central Thrust (MCT), which separates the High Himalayas and the Lesser Himalayas is not well known. Estimates range from the Oligocene [51] to mid-Miocene (e.g. [44]). Most Miocene estimates

are based on K-Ar cooling ages of micas from metamorphic rocks associated with the MCT [44,60 and references therein] or the oldest Siwalik molasse sedimentation [61]. These events are likely to be displaced in time from the beginning of thrusting and related metamorphism. Intracontinental underthrusting of buoyant continental material beginning at 20 Ma could have provided the vertical force needed to drive the rapid uplift of the Gangdese belt to the north of the MCT. Rapid uplift at 20–17 Ma is also consistent with down-to-the-north late Oligocene/early Miocene [62] normal faulting in the Himalayas [63], suggested to be a gravitational collapse feature due to crustal thickening and uplift generated by the accumulated movement of the MCT [64]. Preliminary $^{40}Ar/^{39}Ar$ data from the Himalayas indicate that parts of the High Himalayas were at similar levels of the crust and were experiencing similar uplift to that of the Quxu granodiorite at this time [65].

6. Conclusions

(1) Parts of southern Tibet experienced a marked pulse of uplift to a peak value of about 4 mm/year in the early Miocene.

(2) The Tibetan plateau has not experienced steady uplift over the entire plateau but rather discrete pulses of uplift variable in both space and time.

(3) The main mechanisms that permit accommodation of the convergence of India and Asia have varied significantly in their contribution since the collision started. The samples analyzed are consistent with the suggestion that tectonic escape dominated during the opening of the South China Sea 32 to 17 Ma ago.

(4) The data do not support crustal thickening models in which Indian continental crust progressively and directly underthrusts Asian crust and are also not consistent with very young uplift that would be required by delayed rise of subducted Indian continental crust. The data are consistent, so far as they go, with distributed shortening for thickening the crust of the Tibetan plateau over the past ca. 20 Ma.

Acknowledgements

We thank P. England and D. Seidemann and two anonymous French gentlemen for helpful reviews. We thank Don Baker for help with the hydrothermal experiment on biotite. W.K. thanks Mr. Len Mole (Royal Society of London staff) for accompanying him on the sampling traverse from 3600 to 4600 meters ASL after only three days at high altitude and Biman Bangladesh Airlines for not losing the bag with the samples in it. The samples were collected during the Geotraverse of the Tibetan Plateau sponsored by the Academia Sinica and the Royal Society; funding for W.K.'s participation provided by National Science Foundation grant EAR 84-17640 and NASA grant NAG-G5-524.

References

1 A. Nicolas and 7 others, The Xigaze ophiolite (Tibet): a peculiar oceanic lithosphere, Nature 294, 414–417, 1981.
2 Tu G., Zhang Y., Zhao Z. and Wang Z., Characteristics and evolution of granitoids of southern Xizang, in: Proceedings of Symposium on Qinghai-Xizang (Tibet) Plateau, Vol. 1. Geology, Geological History and Origin of Qinghai Xizang Plateau, pp. 353–361, 1981.
3 F. Debon, P. LeFort, S.M.F. Sheppard and J. Sonet. The four plutonic belts of the Transhimalaya-Himalaya: a chemical, mineralogical, isotopic, and chronological synthesis along a Tibet-Nepal section, J. Petrol. 21, 219–250, 1986.
4 U. Schärer, Xu R.-H. and C.J. Allègre. U-Pb geochronology of the Gangdese (Transhimalaya) plutonism in the Lhasa-Xigaze region, Tibet, Earth Planet. Sci. Lett. 69, 311–320, 1984.
5 Xu R.-H., U. Schärer and C.J. Allègre. Magmatism and metamorphism in the Lhasa block (Tibet): a geochronological study, J. Geol. 93, 41–57, 1985.
6 P. Molnar and P. Tapponnier, Cenozoic tectonics of Asia: effects of a continental collision, Science 189, 419–426, 1975.
7 J. Besse, V. Courtillot, J.P. Pozzi, M. Westphal and Zhou, Y.X., Paleomagnetic estimates of crustal shortening in the Himalayan thrusts and Zangbo suture, Nature 311, 621–626, 1984.
8 P. Patriat and J. Achache, India-Eurasia collision chronology has implications for crustal shortening and driving mechanism of plates, Nature 311, 615–621, 1984.
9 J. Achache, V. Courtillot and Zhou Y.X., Paleogeographic and tectonic evolution of southern Tibet since Middle Cretaceous time: new paleomagnetic data and synthesis, J. Geophys. Res. 89, 10,311–10,339, 1984.
10 C.T. Klootwijk, Greater India's northern extent and its underthrust of the Tibetan plateau: paleomagnetic con-

straints and implications, in: Zagros, Hindu Kush, Himalaya Geodynamic Evolution, H.K. Gupta and F.J. Delany, eds., Am. Geophys. Union, Geodyn. Ser. 3, 313–323.
11 J.F. Dewey and K.C.A. Burke, Tibetan, Variscan and Precambrian basement reactivation: products of continental collision, J. Geol. 81, 683–692, 1973.
12 K. Burke and J.F. Dewey, Orogeny in Africa, in: African Geology, T.F. Dessanvagie and A.J. Whiteman, eds., pp. 583–608, University of Ibadan Press, 1972.
13 P. Molnar and P. Tapponnier, Active tectonics of Tibet, J. Geophys. Res. 83, 5361–5375, 1978.
14 K. Burke and C. Sengor, Tectonic escape in the evolution of the continental crust, in: Reflection Seismology: The Continental Crust, Am. Geophys. Union, Geodyn. Ser. 14, 41–53, 1986.
15 R. Armijo, P. Tapponnier, J.L. Mercier and Han Tong-Lin, Quaternary extension in southern Tibet: field observations and tectonic implications, J. Geophys. Res. 91, 13,803–13,872, 1986.
16 T.M. Harrison and J.D. FitzGerald, Exsolution in hornblende and its consequences for $^{40}Ar/^{39}Ar$ age spectra and closure temperature, Geochim. Cosmochim. Acta 50, 247–253, 1986.
17 M.H. Dodson, Closure temperature in cooling geochronological and petrological systems, Contrib. Mineral. Petrol. 40, 259–274, 1973.
18 B.J. Giletti, Diffusion related to geochronology, in: Geochemical Transport and Kinetics, Hoffman et al., eds., Carnegie Inst. Washington Publ. 634, 61–76, 1975.
19 T.M. Harrison, I.J. Duncan and I. McDougall, Diffusion of ^{40}Ar in biotite: temperature, pressure and compositional effects, Geochim. Cosmochim. Acta 49, 2461–2468, 1985.
20 T.M. Harrison and I. McDougall, The thermal significance of potassium feldspar K-Ar ages inferred from $^{40}Ar/^{39}Ar$ age spectrum results, Geochim. Cosmochim. Acta 46, 1811–1820, 1982.
21 S.L. Baldwin, T.M. Harrison and K. Burke, Fission track evidence for the source of accreted sandstones, Barbados, Tectonics 5, 457–468, 1986.
22 C.W. Naeser, Fission track dating, U.S. Geol. Surv., Open File Rep. 76-190, 66 pp., 1976.
23 C.W. Naeser, R.A. Zimmerman, and G.T. Cebular, Fission track dating of apatite and zircon: an interlaboratory comparison, Nucl. Tracks 5, 65–72, 1981.
24 C.J. Allègre and 34 others. Structure and evolution of the Himalayan-Tibet orogenic belt, Nature 307, 17–22, 1984.
25 Zhang Y., Wang Z., Zhao Z., Xu Y., Lin X. and Xie Y., On the crustal movement characteristics of the Xizang Plateau with special reference to intermediate-acid magmatic activities, in: Proceedings of Symposium on Qinghai-Xizang (Tibet) Plateau, Vol. 1. Geology, Geological History and Origin of the Qinghai-Xizang Plateau, pp. 427–432, 1981.
26 N.B.W. Harris, Xu R., C.L. Lewis, C.J. Hawkesworth and Zhang Y., Isotope geochemistry of the Tibetan Plateau, Philos. Trans. R. Soc. London, in press, 1987.
27 J.M. Hammerstrom and E. Zen. Aluminum in hornblende: an empirical igneous geobarometer, Am. Mineral. 71, 1297–1313, 1986.
28 L. Hollister, G.C. Grissom, E.K. Peters, H.H. Stowell and V.B. Sisson, Confirmation of the empirical correlation of Al in hornblende with pressure of solidification of calc-alkaline plutons, Am. Mineral. 72, 231–239, 1987.
29 T.M. Harrison and M. Heizler, Multiple trapped Argon isotopic components revealed by $^{40}Ar/^{39}Ar$ isochron analysis, EOS 68, 431, 1987.
30 K.A. Foland, ^{40}Ar diffusion in homogeneous orthoclase and an interpretation of Ar diffusion in K-feldspar, Geochim. Cosmochim. Acta 38, 151–166, 1974.
31 D.D. Blackwell, The thermal structure of the continental crust, in: The Structure and Physical Properties of the Earth's Crust, J.G. Heacock, ed., Am. Geophys. Union, Geophys. Monogr. Ser. 14, 169–184, 1971.
32 T.M. Harrison and G.K.C. Clarke, A model of the thermal effects of igneous intrusion and uplift as applied to Quottoon pluton, British Columbia, Can. J. Earth Sci. 16, 411–420, 1979.
33 R.A. Haugerud, 1DT—an interactive, screen oriented microcomputer program for simulation of 1-dimensional geothermal histories, U.S. Geol. Surv., Open File Rep. 86-511, 16 pp., 1986.
34 C.W. Naeser, The fading of fission tracks in the geologic environment—data from deep drill holes, Nucl. Tracks 5, 248–258, 1981.
35 T.M. Harrison, A reassessment of fission-track annealing behavior in apatite, Nucl. Tracks 10, 329–333, 1985.
36 P. Tapponnier, G. Peltzer and R. Armijo, On the mechanics of the collision between India and Asia, in: Collision Tectonics, M.P. Coward and A.C. Ries, eds., Geol. Soc. London, Spec. Publ., 19, 115–157, 1986.
37 A. Hirn and 11 others, Crustal structure and variability of the Himalayan border of Tibet, Nature 307, 23–25, 1984.
38 A. Hirn and 7 others, Lhasa block and bordering suture—a continuation of a 500-km Moho traverse through Tibet, Nature 307, 25–27, 1984.
39 Chang C. and 26 others, Preliminary conclusions of the Royal Society and Academia Sinica 1985 geotraverse of Tibet, Nature 323, 501–507, 1986.
40 P. Molnar, B.C. Burchfiel, Liang K. and Zhao, Z., Geomorphic evidence for active faulting in the Altyn Tagh and northern Tibet and qualitative estimates of its contribution to the convergence of India and Eurasia, Geology 15, 249–253, 1987.
41 E. Argand, La tectonique de l'Asie, Proc. 13th Int. Geol. Congr. 7, 171–372, 1924.
42 C.McA. Powell and P.C. Conaghan, Plate tectonics and the Himalayas, Earth Planet. Sci. Lett. 20, 1–12, 1979.
43 P. Bird, Initiation of intracontinental subduction in the Himalaya, J. Geophys. Res. 83, 4975–4987, 1978.
44 C.McA. Powell, Continental underplating model for the rise of the Tibetan Plateau, Earth Planet. Sci. Lett. 81, 79–94, 1986.
45 Zhao W. and W.J. Morgan, Uplift of the Tibetan Plateau, Tectonics 4, 359–369, 1985.
46 Zhao W. and W.J. Morgan, Injection of Indian crust into Tibetan lower crust: a two-dimensional finite element model study, Tectonics 4, 489–504, 1987.
47 Zhao W. and D.A. Yuen, Injection of Indian crust into

Tibetan lower crust: a temperature-dependent viscous model, Tectonics 4, 505–514, 1987.
48 P.K. Zeitler, Cooling history of the NW Himalaya, Pakistan, Tectonics 4, 127–151, 1985.
49 C. Coulon, H. Maluski, C. Bollinger and S. Wang, Mesozoic and Cenozoic volcanic rocks from central and southern Tibet: ^{39}Ar-^{40}Ar dating, petrological characteristics and geodynamical significance, Earth Planet. Sci. Lett. 79, 281–302, 1986.
50 J.P. Burg, F. Proust, P. Tapponnier and G.M. Chen, Deformation phases and tectonic evolution of the Lhasa block (southern Tibet, China), Eclogae Geol. Helv. 76, 643–665, 1983.
51 R.M. Shackleton, Structure of southern Tibet: Report on a traverse from Lhasa to Kathmandu organized by Academia Sinica, J. Struct. Geol. 3, 97–105, 1981.
52 A. Gansser, The Geology of the Himalaya, 289 pp., Wiley-Interscience, New York, N.Y., 1964.
53 Xu S., The evolution of the paleogeographic environments in the Tanggula Mountains in the Pliocene-Quaternary, in: Geological and Ecological Studies of Qinghai-Xizang Plateau, Vol. 1, pp. 247–255, 1981.
54 Xu R., Vegetational changes in the past and the uplift of Qinghai-Xizang plateau, in: Proceedings of Symposium on Qinghai-Xizang (Tibet) Plateau, Vol. 1. Geology, Geological History and Origin of Qinghai-Xizang Plateau, pp. 139–141, 1981.
55 Chen W., Natural environment of the Pliocene Basin in Gyiron Xizang, in: Proceedings of Symposium on Qinghai-Xizang (Tibet) Plateau, Vol. 1. Geology, Geological History and Origin of the Qinghai-Xizang Plateau, pp. 343–352, 1981.
56 Li J., Li B., Wang F., Zhang Q., Wen S. and Zhang B., The process of the uplift of the Qinghai-Xizang plateau, in: Proceedings of the Symposium on Qinghai-Xizang (Tibet) Plateau, Vol. 1. Geology, Geological History and Origin of the Qinghai-Xizang Plateau, pp. 111–118, 1981.
57 Li T., Xiao X., Li G., Gao Y. and Zhou W., The crustal evolution and uplift of the Qinghai-Tibet plateau, Tectonophysics 127, 279–289, 1986.
58 Guo S.-X., On the elevation and climatic changes of the Qinghai-Xizang plateau based on fossil angiosperms, in: Geological and Ecological Studies of Qinghai-Xizang Plateau, Vol. 1, pp. 201–206, 1981.
59 P. Tapponnier, G. Peltzer, A.Y. Le Dain, R. Armijo and P. Cobbold, Propagating extrusion tectonics in Asia: new insights from simple experiments with plasticine, Geology 10, 611–616, 1982.
60 P. LeFort, Metamorphism and magmatism during the Himalayan collision, in: Collision Tectonics, M.P. Coward and A.C. Ries, eds., Geol. Soc. London, Spec. Publ. 19, 159–172, 1986.
61 A. Gansser, The geodynamic history of the Himalaya, in: Zagros, Hindu Kush, Himalaya Geodynamic Evolution, H.K. Gupta and F.M. Delany, eds., Am. Geophys. Union, Geodyn. Ser. 3, 111–121, 1981.
62 P. Copeland, T.M. Harrison, R. Parrish, B.C. Burchfiel, K. Hodges and W.S.F. Kidd. Constraints on the age of normal faulting, north face of Mt. Everest: implications for rapid Oligo-Miocene uplift, EOS, submitted, 1987.
63 J.P. Burg, M. Brunel, D. Gapais, Chen G.M., and Lin G.H., Deformation of leucogranites of the crystalline Main Central Sheet in southern Tibet (China), J. Struct. Geol. 6, 535–542, 1984.
64 B.C. Burchfiel and L.H. Royden, North-south extension within the convergent Himalayan region, Geology 13, 679–682, 1985.
65 P. Copeland, T.M. Harrison, W.S.F. Kidd and Xu R., unpublished data.
66 Ministry of Geology, Geologic Map of Tibet, 1:1,500,000, 8 sheets, Beijing, 1980.
67 J.P. Burg, Carte géologique du sud du Tibet, I.N.A.G., C.N.R.S., Paris, Ministry of Geology, Beijing, 1:500,000, 1983.